NANOPARTICLE SEPARATION AND METROLOGY BY THREE-DIMENSIONAL NANOFLUIDIC SIZE EXCLUSION

S.M. Stavis, J. Geist, and M. Gaitan*
Semiconductor Electronics Division, National Institute of Standards and Technology, USA

ABSTRACT

A nanofluidic approach to the size separation and metrology of nanoparticles by three-dimensional (3D) nanofluidic size exclusion is presented. This approach is fundamentally different from serial methods of nanoparticle purification (*i.e.* filtration) and characterization (*i.e.* electron microscopy); 3D nanofluidic devices enable the parallel actuation and sensing of a mixture of nanoparticles of different sizes by three-dimensional nanofluidic size exclusion. In this manuscript, the design, fabrication and characterization of a 3D nanofluidic device is described in detail. The preliminary application of this 3D nanofluidic device to the size separation and metrology of nanoparticles is introduced.

INTRODUCTION

Nanoparticles are of immense scientific and technological interest, and nanoparticle size often determines the beneficial or detrimental characteristics of nanoparticles. However, current technology for nanoparticle size processing and characterization is a bottleneck to the study and application of many types of nanoparticles [1]. Conventional methods of nanoparticle size separation and purification (*i.e.* filtration) can be slow and inefficient. These limitations are compounded by the subsequent use of conventional methods of nanoparticle characterization (*i.e.* electron microscopy) which can be slow and specialized.

Engineered nanofluidic devices provide microsystem scaling benefits while simultaneously facilitating control and visualization of nanoscale interactions with nanoparticles. These interactions are typically controlled through the confinement of nanoparticles within an engineered nanometer scale fluidic structure and visualized with fluorescence microscopy. However, the vast majority of nanofluidic structures have been characterized by simple geometries defined by at most several structure depths. This has limited the range and resolution of nanofluidic approaches to the manipulation and metrology of nanoparticles. As nanofluidic device functionality is determined by nanofluidic structure dimensionality and complexity, the development of more complex three dimensional nanofluidic structures would confer improved control over interactions with nanoparticles. This could result in new nanofluidic technologies for the manipulation and metrology of nanoparticles [2]. Progress in this regard has been restricted by conventional nanofabrication processes, which become limiting if many layers of lithography are performed in a research nanofabrication facility.

In this manuscript, a nanofluidic technology is presented to address these limitations. A nanofabrication process is described to construct nanofluidic devices with numerous nanometer-scale critical dimensions. In aggregate, these numerous critical device dimensions form a complex three-dimensional surface enabling the simultaneous on-chip actuation and sensing of nanoparticles of different sizes. The preliminary application of a 3D nanofluidic device to the size separation and metrology of a mixture of nanoparticles of different sizes is introduced.

THEORY

To fabricate nanofluidic devices with numerous nanometer-scale critical dimensions, grayscale photolithography is used in conjunction with a nanometer-scale pattern transfer process. As shown in Figure 1, a chromium-on-quartz photomask is used with a projection photolithography system (*i.e.* a wafer stepper) as a diffraction filter [3, 4]. The photomask is patterned with arrays of

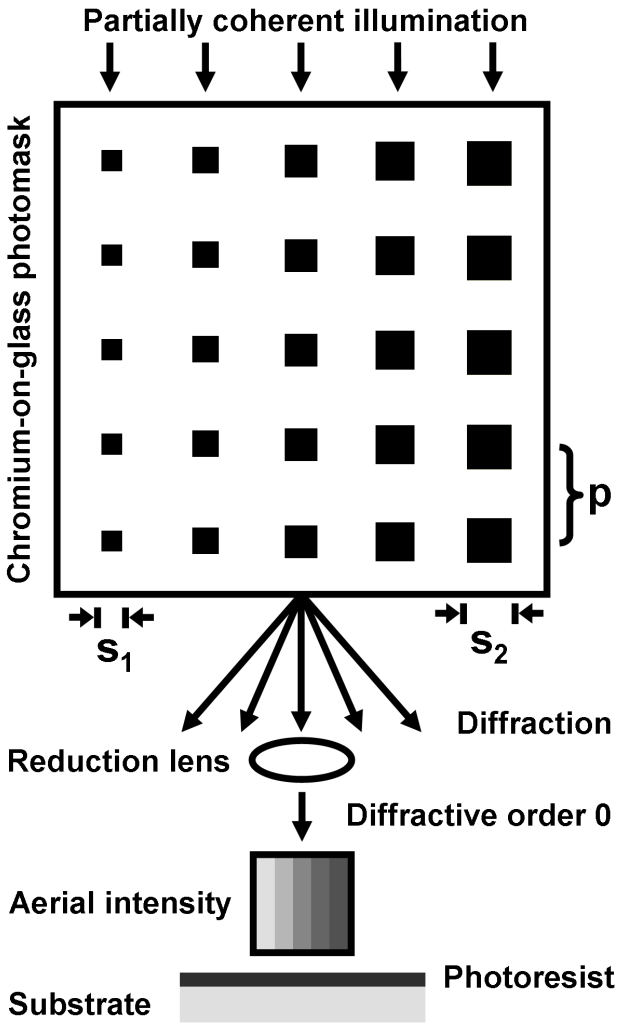

Figure 1: Schematic of a chromium-on-quartz photomask used in conjunction with a reduction photolithography system as a diffraction filter to pattern grayscales of varied intensity.

diffractive chromium squares of size s and pitch p, with amplitude transmittance $T(x,y)$ of 0 and 1 for chromium and quartz regions. The photomask is illuminated with light of wavelength λ and coherence parameter σ, and the lithographic system projects and reduces the device pattern through the lithographic lens and onto a fused silica substrate wafer. For a diffraction-limited optical system, $T(x,y)$ and its Fourier spectrum in the image plane $T'(k_x,k_y)$ are related as conjugates:

$$T(x,y) = \frac{1}{(2\pi)^2}\iint T'(k_x,k_y)e^{-i(k_x x + k_y y)}dk_x dk_y \qquad (1)$$

$$T'(k_x,k_y) = \iint T(x,y)e^{i(k_x x + k_y y)}dxdy \qquad (2)$$

with lateral components of the angular wave number $k_x=(2\pi/\lambda)\sin\alpha$ and $k_y=(2\pi/\lambda)\sin\beta$, and projected angles α and β between the wave vector k and the optical axis. With appropriate selection of *s* and *p*, diffractive orders other than $k_x=k_y=0$ are rejected by the lens aperture. As the zeroth diffractive order determines only the amplitude of the image intensity, individual elements within the diffractive arrays are not resolved, and a grayscale of uniform intensity results. The critical angle θc for entry into the lens is determined by its numerical aperture $NA_S=\sin\theta_c$, giving a critical wave vector number $k_c=(2\pi/\lambda)NA$. The complex amplitude of the aerial image is then

$$A(x',y') = \int_{-k_c}^{k_c}\int_{-k_c}^{k_c} T'(k_x,k_y)\cdot e^{i(k_x x' + k_y y')}dk_x dk_y \qquad (3)$$

and the aerial image intensity is $I(x',y')=|A(x',y')|^2$. Taking into account the partial coherence of the illuminator, the stepper resolution determines the critical aerial pitch

$$p_c' = \frac{1}{1+\sigma_S}\cdot\frac{\lambda_S}{NA_S} \qquad (4)$$

while the diagonal spacing between adjacent elements in the diffractive array determines the critical square size [5]

$$s_c = p\cdot\sqrt{\frac{p_c^2}{2}} \qquad (5)$$

Pitches larger than p_c or squares smaller than s_c will result in fluctuations in aerial intensity as diffractive elements begin to resolve. When equations (4) and (5) are satisfied, $k_x=k_y=0$ and $T'(k_x,k_y)$ is given in equation (2) as the integral of $T(x,y)$, which is the fractional opaque area of each grayscale on the photomask. The aerial image intensity of a grayscale is then

$$I_{GS}(x',y') = I_0\left(1-\left(\frac{s^2}{p^2}\right)\right)^2 \qquad (6)$$

where I_0 is the incident illumination intensity.

RESULTS

An aerial intensity profile approximated by a staircase function with thirty steps was patterned using arrays of diffractive chromium squares varied in size from s=1.37 μm to s=2.24 μm on a pitch p=4.00 μm. The square sizes had a tolerance of 15 nm (absolute error) and a uniformity of 15 nm (maximum range), as specified by the manufacturer. Each grayscale had an aerial width w_{GS}=4.00 μm, defined by a sub-array on the photomask of five diffractive chromium squares. The intensity of each grayscale I_{GS} in the aerial plane (normalized by the incident illumination intensity I_0), as calculated using Equation 6, is shown as a function of diffractive square size *s* in Figure 2. This range of chromium square sizes were selected to produce an approximately response variation in grayscale intensity, as shown by the corresponding fit. This linear relationship simplified the subsequent design of the nanofabrication process.

A fused silica substrate wafer with thickness t_s=0.50 mm and surface roughness r_s<5 Å was vapor primed and spin-coated with 1.07 μm of broadband positive tone photoresist. The photomask was used with a reduction photolithography tool of magnification M_s=0.2, wavelength λ_s=436 nm, coherence parameter σ=0.43, and numerical aperture NA_S=0.3 to render grayscales for the partial top-down exposure of the photoresist thin film. The photoresist was then fully developed using a positive tone developer. Prior to

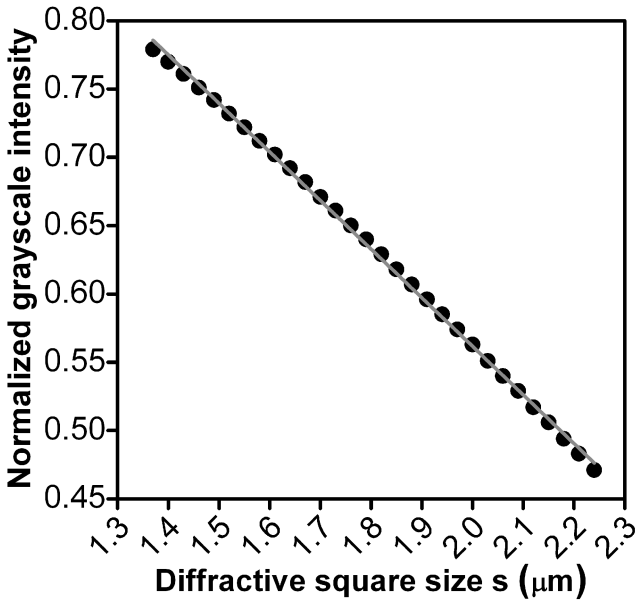

Figure 2: Normalized grayscale intensity (I_{GS}/I_0) *as a function of diffractive chromium square* s. *Square sizes were selected to produce an approximately linear variation in grayscale intensity.*

fabrication of the device presented here, a calibration photomask was used to characterize the response of the photoresist film to grayscale exposure, the results of which are shown in Figure 3. The incident illumination intensity I_0 was the illumination intensity required to produce an exposure dose that completely cleared the photoresist etch mask during the subsequent development process.

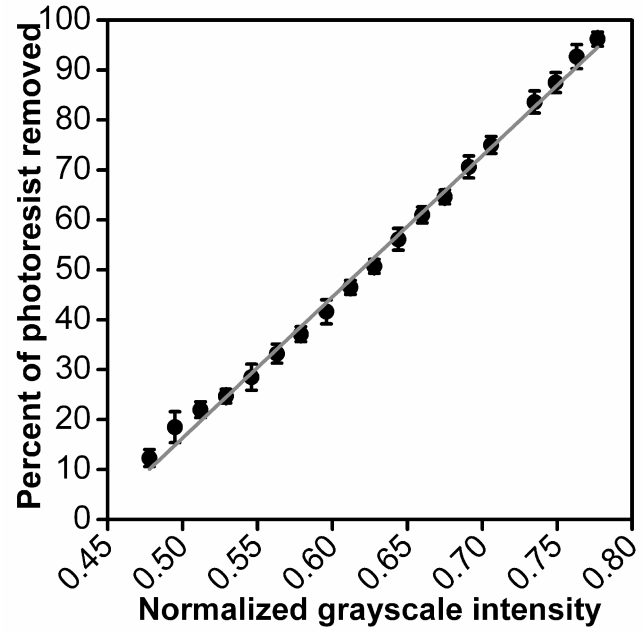

Figure 3: Response of photoresist to grayscale exposure following development. The photoresist responds in an approximately linear manner across the selected range of grayscale intensities.

Following photolithography, the 3D device pattern in the photoresist etch mask was transferred into the fused silica substrate

at the nanometer length scale by an isotropic CHF_3/O_2 reactive ion etch process. The selectivity of the etch process was tuned by varying the two gas flow rates to achieve the desired etch depth profile. Following the pattern transfer process, the resulting 3D topography of the etched surface of the nanofluidic channel was spatially mapped with a scanning probe surface profilometer. The results of this measurement are shown in Figure 4. The radius of curvature of the surface profilometer probe tip was ≈1 μm, as determined by measurement artifacts (*i.e.* rounded corners) that resulted from the probe tip scanning over sharp nanofluidic step edges. Surface profilometry provided the minimum etch depth of the nanofluidic channel, since the micrometer-scale profilometer tip was not able to probe surface roughness at the nanometer-scale. Etch depth variation was controlled to within 10 nm (standard deviation) over the entire 1.2 cm channel length, as measured by 13 scanned probe measurements repeated along the length of the structure. This variation encompassed all of the non-uniformity in the nanofabrication process as implemented, including variation in initial patterning of the photomask, grayscale exposure, photoresist development, and reactive ion etching. The channel had an average minimum depth of ≈70 nm, an average maximum depth of ≈620 nm, and an average step size of ≈18 nm. A fabrication

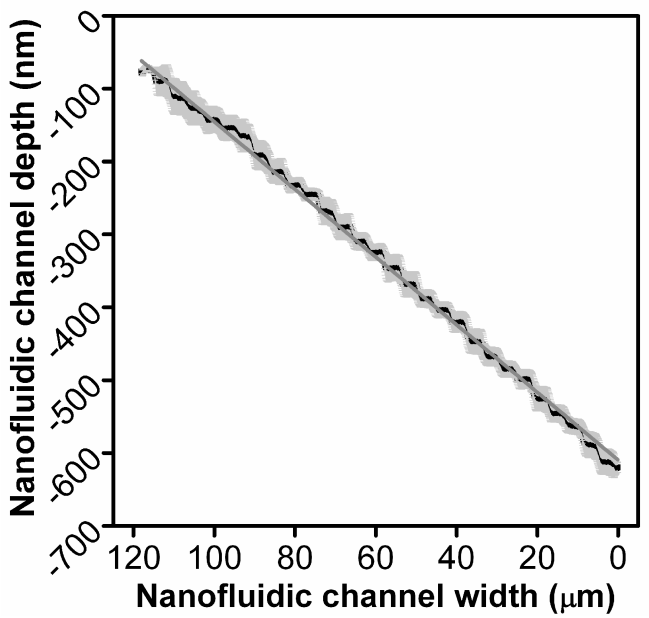

Figure 4: Numerous (30) nanometer-scale etch depths as measured by scanning probe surface profilometry. Error bars denote the standard deviation of 13 scans down the length of the etched channel structure. The etch depth profile of the device is approximated by a staircase function which demonstrates the linearity of the nanofabrication process from grayscale exposure to photoresist response to pattern transfer.

process defect resulted in periodic distortions of the nominal staircase function depth profile, as shown in Figure 4. These distortions produced regions of the structure with increased variation in etch depth. The root-mean-square roughness of the etched channel surface was measured with atomic force microscopy to be ≈2 nm. The radius of the curvature of the etched single crystal silicon probe tip was ≤10 nm, as specified by the manufacturer, and the tip was operated in tapping mode.

Inlet and outlet holes were micro-abrasive blasted through the back of the substrate wafer, which was then cleaned and bonded to a fused silica cover wafer with thickness t_c=0.17 mm and surface roughness r_s<5 Å. The wafer stack was fused at 1100 ˚C. No nanoglassblowing occurred [6], as determined by scanned probe measurements of the cover wafer surface after this annealing process. This measurement (not shown) confirms that the etch depths measured to prior wafer bonding accurately represent the resulting nanofluidic channel depths after wafer bonding.

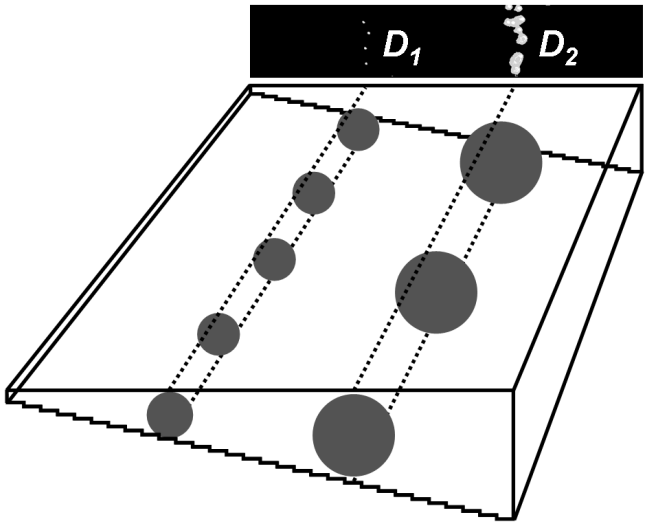

Figure 5: Fluorescence micrograph and schematic showing the size separation of nanoparticles with sizes D_1 and D_2 by three-dimensional nanofluidic size exclusion. Nanoparticles were electrokinetically driven down the length of the nanofluidic channel and across its width from the deep side towards the shallow side. The stepped reductions in nanofluidic channel depth excluded nanoparticles from spatially separate regions of the channel.

Following device fabrication, reservoirs were attached to the substrate to introduce nanoparticle samples into the 3D structure. An aqueous solution of fluorescent nanoparticles of sizes D_1 and D_2 was injected into the deep end of the nanofluidic channel and electrokinetically driven down the length and across the width of the 3D nanofluidic channel from the deep side towards the shallow side, as shown in Figure 5. Stepped reductions in the depth of the nanofluidic channel excluded nanoparticles by size from regions of the nanofluidic channel with depths that were less than the particle sizes, as shown by a fluorescence micrograph at the top of Figure 5. Future work will use epifluorescence microscopy to map the size exclusion positions of numerous individual nanoparticles to corresponding nanofluidic channel depths. This statistical analysis will be used to directly measure the nanoparticle size distributions in order to validate the size separation mechanism of three-dimensional nanofluidic size exclusion.

DISCLAIMER

NOTE

Certain commercial materials and equipment are identified in order to adequately specify experimental procedures. In no case does such identification imply recommendation or endorsement by the National Institute of Standards and Technology, nor does it imply

that the items identified are necessarily the best available for the purpose.

ACKNOWLEDGEMENTS

This research was performed while S.M. Stavis held a National Research Council Research Associateship Award at the National Institute of Standards and Technology (NIST). Device fabrication was performed at the Cornell Nanoscale Science and Technology Facility (CNF), a member of the National Nanotechnology Infrastructure Network, and the Cornell Center for Materials Research, both supported by the NSF. Device characterization was performed in part at the NIST Center for Nanoscale Science and Technology. The authors thank the CNF staff for assistance with device fabrication.

REFERENCES

[1] E.K. Richman and J.E. Hutchison, "The Nanomaterial Characterization Bottleneck", ACS Nano, 3, 9, (2009).

[2] S.M. Stavis, E. A. Strychalski, and M. Gaitan, "Nanofluidic structures with complex three-dimensional surfaces", Nanotechnology, 20, 7 (2009).

[3] W. Henke, W. Hoppe, H. J. Quenzer, P. Staudtfischbach, and B. Wagner, "Simulation and process design of gray-tone lithography for the fabrication of arbitrarily-shaped surfaces", Japanese Journal Of Applied Physics Part 1 – Regular Papers Short Notes & Review Papers, 33, 12B (1994).

[4] J. W. Goodman, Introduction To Fourier Optics, Third Ed., Mcgraw-Hill, 2004.

[5] C. M. Waits, A. Modafe, and R. Ghodssi, "Investigation of gray-scale technology for large area 3D silicon MEMS structures", Journal Of Micromechanics And Microengineering, 13, 170 (2003).

[6] E. A. Strychalski, S. M. Stavis, and H. G. Craighead, "Non-planar nanofluidic devices for single molecule analysis fabricated using nanoglassblowing", Nanotechnology, 19, 8 (2008).

CONTACT

*S.M. Stavis, tel: +1-301-975-3246; sstavis@nist.gov